Journal of Peptide Science
J. Pept. Sci. 2008; **14**: 819–829
Published online 25 January 2008 in Wiley InterScience (www.interscience.wiley.com). DOI: 10.1002/psc.1009

JOURNAL OF PEPTIDE SCIENCE

Solution conformations of bradykinin antagonists modified with Cα–Cα cyclized nonaromatic residues

EMILIA SIKORSKA* and SYLWIA RODZIEWICZ-MOTOWIDŁO
Faculty of Chemistry, University of Gdańsk, Sobieskiego 18, 80-952 Gdańsk, Poland

Received 13 November 2007; Accepted 20 November 2007

Abstract: The conformations of four BK antagonists, [D-Arg^0, Hyp^3, Thi^5, D-Phe^7, Acc^8]BK (**1**), Aaa[D-Arg^0, Hyp^3, Thi^5, D-Phe^7, Acc^8]BK (**2**), [D-Arg^0, Hyp^3, Thi^{5,8}, Apc^7]BK (**3**), and Aaa[D-Arg^0, Hyp^3, Thi^{5,8}, Apc^7]BK (**4**) were studied by using 2D NMR spectroscopy and MD simulations with time-averaged (TAV) restraints. According to the results of the NMR measurements, the BK antagonists contain 7–30% of minor conformation resulting from *cis*/*trans* isomerization of the peptide bonds preceding either Pro or Hyp residues. The major conformation of each peptide possesses all peptide bonds in *trans* configuration. Peptides modified with the Apc residue at position 7 (peptides **3** and **4**) possess a higher percentage of minor isomer.

Peptide **1** exhibits the strongest vasodepressor potency among the analogs studied and as a single one forms the βII-turn in the 2–5 fragment, which is believed to be crucial for antagonistic activity. This peptide is also the most compact. The radius of gyration (Rg) amounts to 6.9 Å and is by *ca* 1.5 Å lower than that of the remaining analogs. With peptide **4**, the ST-turn of type I within the Ser^6-Thi^8 fragment was found. Copyright © 2008 European Peptide Society and John Wiley & Sons, Ltd.

Keywords: bradykinin; bradykinin antagonists; MD; NMR; time-averaged (TAV)

INTRODUCTION

Bradykinin (BK) (Arg^1-Pro^2-Pro^3-Gly^4-Phe^5-Ser^6-Pro^7-Phe^8-Arg^9) is a biologically active nonapeptide resulting from proteolytic action of the plasma kallikrein on a high-molecular-weight kininogen. Additionally, BK may be produced by removal of the amino-terminal Lys of kallidin (KD) (Lys^1-Arg^2-Pro^3–Pro^4-Gly^5-Phe^6-Ser^7-Pro^8-Phe^9-Arg^{10}) by plasma aminopeptidases [1,2]. BK is implicated in a number of physiological and pathophysiological processes. It plays a key role in inflammatory diseases and allergic reactions. Moreover, it mediates some vital processes such as hypotension, smooth muscle, edema, pain, or cell growth [3,4].

The biological effects of BK are mediated by two different types of G-protein coupled receptors (GPCRs), B1 and B2. B1 receptor is expressed under stress conditions such as shock or inflammation, whereas B2 is expressed constitutively [5,6]. B2 receptors require the entire BK sequence for recognition, while B1 receptors recognize and bind only des-Arg^9-BK (formed by kininase I from BK) [7–9].

Naturally occurring kinins (BK and KD) are characterized by very short half-lives, which is a result of kininases action [10,11]. Therefore, searching for new analogs focuses on extension of analog action by increasing their enzymatic tolerance, enhancing activity, and reducing conformational freedom. Moreover, involvement of BK in inflammation and pain is the reason for searching novel active antagonists [12].

It has been demonstrated that a simple change from Pro^7 to D-Phe^7 affords an analog with weak antagonistic properties [13]. Investigations on the structure–activity relationship confirmed also that the replacement of Pro^3 by Hyp, the substitution of Phe^5 with Thi, and the addition of D-Arg, Aaa or Aca to the *N*-terminal part of the molecule enhanced the antagonistic properties [14–16].

Conformational studies of BK antagonists revealed that turn-like structures involving residues 2–5 and 6–9 might be important for antagonism [17]. Moreover, the structure is very often stabilized by a salt bridge between the guanidine moiety of Arg^1 and the *C*-terminal carboxyl group of Arg^9. The type II and II′ of β-turns at positions 3,4 and 7,8, respectively, occurred mostly in BK antagonists [18–22]. Furthermore, it is known that type II of β-turn may be caused by the proline and hydroxyproline residues. Additionally, in type II of β-turn, position $i+2$ is dominated by glycine, because it most readily adopts the α_L conformation. A high probability of a βII′-turn between residues 6 and 9 is provided by a D-amino acid at position 7 [23–26].

In this article, we present the conformational analysis of four B2 antagonists (Table 1) modified at positions 7 or 8 with Cα–Cα cyclized nonaromatic residues, Apc, or Acc. The Apc residue inserted at position 7 led to a reduction of antagonistic properties in the rat uterus assay or even restored the agonism in the blood pressure test, whereas Acc at position 8

Abbreviations: Aaa, adamantaneacetic acid; Aca, adamantanecarboxylic acid; Acc, 1-aminocyclohexane-1-carboxylic acid; Apc, 1-aminocyclopentane-1-carboxylic acid; Hyp, 4-hydroxy-L-proline; Thi, beta-(2-thienyl)-alanine.

*Correspondence to: Emilia Sikorska, Faculty of Chemistry, University of Gdańsk, Sobieskiego 18, 80-952 Gdańsk, Poland;
e-mail: milka@chem.univ.gda.pl

enhanced antagonistic properties in both tests. In turn, acylation of the *N*-terminus led to the enhancement of the antagonistic potency in blood pressure test only in the case of analogs with Apc at position 7 [27,28]. BK was used as a standard agonist in the activity tests, whereas [D-Arg^0,Hyp^3,Thi^{5,8},D-Phe^7]BK, the B2 antagonist previously synthesized in Stewart's laboratory [13], served as a reference compound for comparison of the antagonistic activities of the analogs in this study [29,30].

Previous theoretical and experimental studies have shown that 1-aminocycloalkane-1-carboxylic acids impart considerable stereochemical rigidity to peptide backbones, which are constrained to adopt conformations in the $3_{10}/\alpha$-helical regions of the φ and ψ spaces. They can be accommodated at either position of type III (III′) β-turn or at the $i+2$ position of type II (II′) β-turn [31–33]. Furthermore, they display the tendency to induce γ- or inverse γ-turn (C_7-conformation) [34].

MATERIALS AND METHODS

Sample Preparation

All the peptides were synthesized by using a procedure described by Labudda *et al.* [27,28] and were of >95% purity. Peptides were dissolved in 90% H_2O/10% D_2O. Samples were prepared using 5.00 mg of each peptide and 0.6 ml of solvent. The pH of the samples fell in the range of 5.0–5.5.

NMR Measurements

The NMR spectra were recorded on a 500 MHz Varian spectrometer equipped with a Performa II gradient generator unit, WFG, Ultrashims, high stability temperature unit and a 5-mm $^1H\{^{13}C/^{15}N\}$ PFG triple resonance inverse probe head.

The 2D NMR spectra were recorded at 30 °C. The temperature coefficients of the amide proton chemical shifts were measured from 1D NMR spectra for the following temperatures: 2, 10, 20, 30, 40, and 50 °C. Proton resonance assignments were achieved by use of the proton–proton TOCSY [35], the NOESY [36], the ROESY [37,38], as well as the gradient heteronuclear single quantum coherence ($^1H-^{13}C$ gHSQC) [39,40] and the gradient heteronuclear multiple quantum coherence ($^1H-^{13}C$ gHMBC) techniques [41]. For each sample, the TOCSY spectra with the mixing time of 80 ms were measured. The NOESY spectra were recorded with a mixing time of 200 ms. The mixing times of the ROESY experiments were set to 200 and 300 ms. The volumes of cross peaks were picked up for ROESY spectra with a mixing time of 300 ms. The calculations were performed only for a more populated conformation of each peptide.

All the spectra were measured with a water signal presaturation pulse typically of 2 dB and 1.5 s. In the case of the 1D NMR spectra, 16 K data points were collected and a spectral width of 6 kHz was used. The 2D homonuclear experiments were measured using a proton spectral width of 4.5 kHz collecting 2 K data points.

Vicinal coupling constants, $^3J_{HNH\alpha}$, were assigned using double quantum filtered-correlation spectroscopy (DQF-COSY) [42] and the 1D NMR spectra. The DQF-COSY spectra were processed to enhance the resolution to 1.2 Hz per point in F2. For Gly, the two $^3J_{HNH\alpha}$ coupling constants with H_α protons are equal within the limits of experimental error.

All chemical shifts are quoted relative to the external 2,2-dimethyl-2-silapentanesulfonic acid (DSS) reference. The ^{13}C chemical shifts were referenced to DSS according to the following relationship: $^{13}C/^1H = 0.251449530$ [43]. Spectral processing was carried out using the VNMR [44] and analyzed with XEASY [45].

MD Calculations

MD simulations were carried out using the AMBER [46] force field. The valence geometry of the residues not specified in the standard AMBER database, were parameterized as recommended by the AMBER 8.0 [46] manual. Specifically, these residues were modeled using bond lengths, the valence

Table 1 The BK analogs and their pharmacological properties

Peptide	Uterotonic potency: % of activity of BK or pA_2	Vasodepressor potency			Ref.
		ED_{20} (mg/min)	ED_{50} (mg/min)	ED_{90} (mg/min)	
[D-Arg^0,Hyp^3,Thi^{5,8},D-Phe^7]BK (Stewart's peptide)	$pA_2 = 6.88 \pm 0.08$	1.73 ± 0.43	—	124.17 ± 27.04	29, 30
1. [D-Arg^0,Hyp^3,Thi^5,D-Phe^7,Acc^8]BK	$pA_2 = 7.2 \pm 0.2$	0.20 ± 0.03	1.62 ± 0.18	25.52 ± 2.15	28
2. Aaa[D-Arg^0,Hyp^3,Thi^5,D-Phe^7,Acc^8]BK	$pA_2 = 7.4 \pm 0.2$	0.66 ± 0.08	4.89 ± 0.36	79 ± 15	28
3. [D-Arg^0,Hyp^3,Thi^{5,8},Apc^7]BK	0.25	13.49 ± 4.25	166.9 ± 63.16	8302 ± 4782	27
4. Aaa[D-Arg^0,Hyp^3,Thi^{5,8},Apc^7]BK	0	2.83 ± 0.36	46.03 ± 12.66	2899 ± 1187	27

Agonistic activity was calculated as percentage of BK activity (set to 100%); antagonistic activity was calculated as pA_2 (negative decadic logarithm of analog concentration shifting the log dose–response curve for BK by a factor of 0.3 to the right: calculations were made from the linear portions of the curves); ED20, ED50, and ED90 represent doses of BK antagonist (μg/kg/min) that inhibit the vasodepressor response to 250 ng of BK by 20, 50, and 90%, respectively.

DOI: 10.1002/psc

and torsion angles of appropriate residue and compatible molecular segments taken from the CSDS database [47]. The point charges were optimized by fitting them to the *ab initio* molecular electrostatic potential (6–31G basis set, GAMESS'98 [48] - *ab initio* molecular electronic structure program) for two different conformations of every nonstandard residue, followed by consecutive averaging the charges over all conformations, as recommended by the RESP protocol [49].

MD calculations were started from extended conformations, which were put into water solution. The initial solvent configuration around the peptide was obtained by filling cubic box with water molecules. The overall box size was enlarged by about 8 Å in each direction. A total number of 1393, 1881, 1166, and 1452 water molecules were used for peptides **1**, **2**, **3**, and **4**, respectively. The chloride ions were used to neutralize the system. To equilibrate the solution density, initial simulations were carried out at 303 K, in a periodic box, until the density was close to 1.0 g/ml.

After equilibration, the MD with time-averaged (TAV) distance and dihedral angle restraints derived from the NMR spectroscopy were performed. The interproton distances were restrained with the force constants $f = 20$ kcal/(mol × Å^2), and the dihedral angles with $f = 2$ kcal/(mol × rad^2). The geometry of the peptide groups was kept fixed according to the NMR data ($f = 50$ kcal/(mol × rad^2)). During MD simulation with TAV, an 8 Å cutoff radius was chosen. The MD simulations were carried out at 303 K in a periodic box of constant volume, with the particle-mesh Ewald (PME) procedure. The time step was 2 fs. The total duration of the run was 4 ns. The coordinates were collected every 2000th step. The conformations obtained during the last 800 ps of simulation were considered in further analysis. As a result, 200 conformations for each peptide were presented.

The interproton distances, used in TAV, were calculated by the CALIBA algorithm of the DYANA [50] program. The macro CALIBA performs calibrations of the cross peaks using three different calibration classes: (i) cross peaks assigned to backbone protons, (ii) cross peaks assigned to more flexible protons of side chains, and (iii) cross peaks assigned to methyl groups. The calibration functions used for these two classes are: $V = A/d^6$, $V = B/d^4$ and $V = C/d^4$, where V is a peak volume and d is the corresponding distance. We used parameter A corresponding to the intensity of cross peak between geminal protons (1.8 Å) for each peptide separately [51]. The scalar B was set to $B = A/d_{\min}{}^2$ in order to intersect the backbone calibration curve at $d_{\min}$, and C set to $C = B/3$ ($d_{\min}$ – minimal value for distance constraints before possible pseudo atom corrections are added).

The backbone $^3J_{\mathrm{HNH}\alpha}$ coupling constants were converted to backbone torsion angle ϕ constraints according to the following rules: $^3J_{\mathrm{HNH}\alpha} < 6$ Hz constrained the ϕ angle to the range of -90° to -30°, 6 Hz $< {}^3J_{\mathrm{HNH}\alpha} < 8$ Hz constrained to the range of -120° to -60°, and $^3J_{\mathrm{HNH}\alpha} > 8$ Hz constrained to the range of -140° to -100° [52].

The results obtained were analyzed using the Carnal and Ptraj programs from the AMBER 8.0 package [46]. Molecular structures were drawn and analyzed with the graphic program MOLMOL [53].

RESULTS

Analysis of NMR Spectra

The NMR spectra of each analog display two distinct sets of proton resonances resulting from two conformations being in equilibrium. Their appearance is probably due to the *cis*/*trans* isomerization of one of the peptide bonds, but this hypothesis has not been supported by appropriate cross peaks. It is more probable that the peptides possess Pro and Hyp at positions 2 and 3, respectively. The percentage of *cis* isomer can be calculated from the nonoverlapping signals of the HN proton of Acc or Apc on the 1D NMR spectra at 30 °C. The contributions of less populated isomer amount from 7% for analogs modified with Acc at position 8 to 30% for those modified with Apc at position 7. The major conformation of each peptide possesses all peptide bonds in *trans* configurations, which was verified by the following cross peaks: H$\alpha(i)$–HN$(i+1)$ and H$\alpha(i)$–H$\delta(i+1)$ in the case of the Pro residue. With the Pro^2–Hyp^3 peptide bond, hydroxyproline Cβ and Cγ chemical shifts were used to distinguish between the *cis* and *trans* peptide bond, because, only for peptide **2**, the H$\alpha(i)$–H$\delta(i+1)$ connectivity for the Pro^2–Hyp^3 peptide bond, which is characteristic of *trans* configuration, was found. It is known that a decreased ^{13}C chemical shift dispersion of Cγ and Cβ in a hydroxyproline residue ($\Delta\delta_{C\gamma—C\beta} \approx 30$ ppm) suggests that the preceding carbonyl is configured in a *cis* peptide bond, while Hyp having a more common *trans* peptide bond shows a larger chemical shift dispersion ($\Delta\delta_{C\gamma—C\beta} \approx 33$ ppm) [54]. The $\Delta\delta_{C\gamma—C\beta}$ dispersions for Hyp^3 are 32.73, 32.83, 32.80, and 32.92 for peptides **1**, **2**, **3**, and **4**, respectively, which is in good agreement with an expected chemical shift dispersion of ≈33 ppm for the *trans* form.

A comparison of the proton and carbon chemical shifts of peptide **1** with **2**, and those of **3** with **4** shows noticeable differences for D-Arg^0 and Arg^1 (Tables 2 and 3), which may suggest appreciable influence of Aaa on three-dimensional structures of the *N*-terminus of peptides **2** and **4**.

The observable NMR parameters such as the ROE connectivities, temperature coefficients, or coupling constants, $^3J_{\mathrm{HNH}\alpha}$, which are diagnostic of secondary structure, are sufficient to identify even quite small populations of reverse structures. The sequential H$\alpha(i)$–HN$(i+1)$ ROE connectivity is always observed and is mostly very strong. Similar, intraresidual H$\alpha(i)$–HN(i) and H$\beta(i)$–HN(i) ROE connectivities are also present for most peptides. In turn, sequential HN(i)–HN$(i+1)$ ROE connectivities are seen only in those regions of the peptides which preferentially adopt folded conformations [55]. In the case of the investigated peptides, intraresidual and sequential connectivities are the main sources of information about secondary structure. First of all, as seen in Figure 1, the H$\alpha(i)$–HN(i) connectivities are much weaker than the

DOI: 10.1002/psc

Table 2 Proton and carbon chemical shifts (ppm) of [D-Arg^0,Hyp^3,Thi^5,D-Phe^7,Acc^8]BK (**1**) and Aaa[D-Arg^0,Hyp^3,Thi^5,D-Phe^7,Acc^8]BK (**2**) in H_2O/D_2O (9 : 1), at 30 °C

Residue	Peptide	Chemical shifts (ppm)					
		CONH	$C_\alpha H$	$C_\beta H$	$C_\gamma H$	$C_\delta H$	Other
Aaa^{-1}	**1**	—	—				—
	2	—	2.04				$H_{2,6,7}$ 1.54; $H_{3,5,8}$ 1.91; $H_{4,9,10}$ 1.69, 1.57
		177.55	52.06				$C_{2,6,7}$ 44.96; $C_{3,5,8}$ 31.07; $C_{4,9,10}$ 38.72
D-Arg^0	**1**	n	4.04	1.92	1.64	3.23	ε-HN 7.24
		172.24	55.63	30.74	26.40	43.16	
	2	8.16	4.27	1.81, 1.71	1.62	3.19	ε-HN 7.20
		176.26	56.19	30.63	27.29	43.02	
Arg^1	**1**	8.85	4.61	1.78, 1.70	1.65	3.13	ε-HN 7.16
		n	54.25	30.05	26.90	43.45	
	2	8.07	4.62	1.76, 1.64	1.56	3.11	ε-HN 7.14
		n	n	30.37	26.93	43.42	
Pro^2	**1**	—	n	2.34, 1.86	2.01	3.86, 3.53	
		174.87	61.73	30.54	27.31	50.53	
	2	—	4.68	2.32, 1.84	1.97	3.79, 3.49	
		174.86	n	30.80	27.31	50.43	
Hyp^3	**1**	—	4.54	2.32, 2.02	4.62	3.83	
		176.89	61.73	39.92	72.65	57.86	
	2	—	4.53	2.31, 2.03	4.62	3.82	
		176.87	61.99	39.83	72.66	57.78	
Gly^4	**1**	8.52	3.93				
		174.09	45.26				
	2	8.54	3.96, 3.90				
		174.18	45.37				
Thi^5	**1**	8.06	4.61	3.34, 3.19			H_2 6.94; H_3 7.34; H_4 7.34
		175.00	57.37	33.56			C_2 129.69; C_3 129.95; C_4 127.90
	2	8.06	4.59	3.34, 3.19			H_2 6.94; H_3 7.02; H_4 7.33
		174.85		33.74			C_2 129.71; C_3 129.94; C_4 127.87
Ser^6	**1**	8.17	4.35	3.67			
		174.33	58.38	63.82			
	2	8.16	4.34	3.67			
		174.28	58.40	63.90			
D-Phe^7	**1**	8.17	4.66	3.17, 2.99			$H_{2,6}$ 7.30; $H_{3,5}$ 7.38; H_4 7.33
		174.85	57.95	39.33			$C_{2,6}$ 131.75; $C_{3,5}$ 131.44; C_4 129.91
	2	8.15	4.66	3.17, 2.99			$H_{2,6}$ 7.30; $H_{3,5}$ 7.41 H_4 7.33
		174.79		39.17			$C_{2,6}$ 131.87; $C_{3,5}$ 131.57; H_4 129.88
Acc^8	**1**	7.85					$H_{2,6}$ 2.00, 1.74; $H_{3,5}$ 1.25,1.15; H_4 1.23, 1.54
		179.32					$C_{2,6}$ 34.12; $C_{3,5}$ 23.30; C_4 27.08
	2	7.84					$H_{2,6}$ 2.00, 1.71; $H_{3,5}$ 1.25, 1.18; H_4 1.52, 1.15
		179.33					$C_{2,6}$ 34.34; $C_{3,5}$ 23.43; C_4 27.11
Arg^9	**1**	7.70	4.32	1.90, 1.73	1.59	3.17	ε-HN 7.13
		n	55.37	30.59	27.23	43.32	
	2	7.66	4.30	1.89, 1.72	1.58	3.18	ε-HN 7.14
		n	55.54	30.54	27.31	43.20	

sequential H$\alpha(i)$–HN$(i+1)$ ones, despite the finding that the H$\alpha(i)$–HN(i) distance is 2.8 Å, which suggests unfolded peptides [56]. The presence of HN(i)–HN$(i+1)$ ROE cross peaks may suggest the reverse structures in the middle part and *C*-terminus of the molecules. With peptide **1**, additional useful information is the spatial proximity of the Hδ protons of Pro^2 to the Hβ ones of Thi^5 and of the Hβ protons of Thi^5 to the HN proton of D-Phe^7. The former may imply β-turn in the 2–5 fragment, whereas the latter shows the possibility of existence of a reverse structure in the middle part of the molecule. Consequently, the medium-range H$\alpha(Aaa^{-1})$–HN(Arg^1) interaction and the long-range H$\alpha(Aaa^{-1})$–HN(Gly^4) one found for peptide **2** indicate that the *N*-terminus is involved in reverse structures. In turn, the ROESY spectra of

DOI: 10.1002/psc

Table 3 Proton and carbon chemical shifts (ppm) of [D-Arg^0,Hyp^3,Thi^{5,8},Apc^7]BK (**3**) and Aaa[D-Arg^0,Hyp^3,Thi^{5,8},Apc^7]BK (**4**) in H_2O/D_2O (9 : 1), at 30 °C

Residue	Peptide	Chemical shifts (ppm)					
		CONH	$C_\alpha H$	$C_\beta H$	$C_\gamma H$	$C_\delta H$	Other
Aaa^{-1}	**3**	—	—				—
	4	—	2.04				$H_{2,6,7}$ 1.55; $H_{3,5,8}$ 1.93; $H_{4,9,10}$ 1.71, 1.60
		177.66	53.03				$C_{2,6,7}$ 45.01; $C_{3,5,8}$ 31.13; $C_{4,9,10}$ 38.83
D-Arg^0	**3**	n	4.04	1.92	1.64	3.23	ε-HN 7.24
		172.50	55.81	31.03	26.69	43.17	
	4	8.16	4.27	1.80, 1.71	1.61	3.19	ε-HN 7.20
		178.15	56.37	30.87	27.14	43.54	
Arg^1	**3**	8.85	4.60	1.77, 1.71	1.64	3.12	ε-HN 7.16
		n	54.35	30.27		43.57	
	4	8.08	4.60	1.74, 1.65	1.55	3.09	ε-HN 7.14
		n	53.67	30.60	26.74	43.54	
Pro^2	**3**	—	4.75	2.35, 1.87	2.02	3.86, 3.52	
		174.84	n	30.85	27.58	50.82	
	4	—	4.69	2.32, 1.85	1.98	3.78, 3.48	
		174.86	61.67	30.73	27.18	50.49	
Hyp^3	**3**	—	4.54	2.31, 2.03	4.62	3.83	
		176.84	61.99	39.94	72.74	58.09	
	4	—	4.53	2.30, 2.02	4.62	3.82	
		177.14	62.06	39.79	72.71	57.79	
Gly^4	**3**	8.54	3.93				
		174.08	45.50				
	4	8.56	3.96, 3.86				
		176.45	45.37				
Thi^5	**3**	8.04	4.60	3.37, 3.28			H_2 7.02; H_3 n; H_4 7.31
		175.17	57.42	33.54			C_2 129.85; C_3 n; C_4 129.96
	4	8.03	4.58	3.37, 3.28			H_2 6.94; H_3 7.03; H_4 7.36
		175.27	57.92	33.33			C_2 129.95; C_3 130.13; C_4 128.17
Ser^6	**3**	8.18	4.33	3.80, 3.74			
		173.93	55.44	64.08			
	4	8.17	4.31	3.79, 3.73			
		174.06	58.25	63.88			
Apc^7	**3**	8.24					$H_{2,5}$ 2.09, 1.85; $H_{3,4}$ 1.91, 1.69
		178.66					$C_{2,5}$ 34.10; $C_{3,4}$ n
	4	8.21					$H_{2,5}$ 2.08, 1.84; $H_{3,4}$ 1.93, 1.69
		178.82					$C_{2,5}$ 39.38; $C_{3,4}$ 26.81
Thi^8	**3**	7.77	4.58	3.34, 3.26			H_2 6.92; H_3 n; H_4 7.33
		174.97		33.58			C_2 129.71; C_3 n; C_4 128.02
	4	7.77	4.57	3.39, 3.25			H_2 6.92; H_3 n; H_4 7.31
		174.27	n	33.31			C_2 129.72; C_3 n; C_4 127.90
Arg^9	**3**	7.97	4.30	1.89, 1.77	1.60	3.18	ε-HN 7.15
		n	56.06	30.57	27.37	43.51	
	4	7.98	4.30	1.88, 1.76	1.59	3.18	ε-HN 7.16
		173.87	55.87	30.82	26.92	43.42	

peptide **3** display only one medium-range connectivity, Hβ(*Hyp*^{3})–HN(*Thi*^{5}), which may influence the formation of a turn structure in the middle part of the peptide. The absence of medium- and long-range interactions in the ROESY spectra of peptide **4** suggests that this peptide exhibits the tendency to assume the most extended conformation among all the peptides studied.

The temperature coefficients of the amide protons ($-\Delta\delta/\Delta T$) fall in the range 5.5–8.9 ppb/K, thus excluding the formation of strong intramolecular hydrogen bonds [57]. Moreover, most of the coupling constant values, $^3J_{HNH\alpha}$, fall in the range 6–8 Hz, which is characteristic of statistical-coil structure [52]. However, these coupling constants do not exclude the possibility of reverse structures, and high temperature coefficients,

DOI: 10.1002/psc

Figure 1 The ROE effects corresponding to their interproton distances, $^3J_{HNH\alpha}$ coupling constants, and the temperature coefficients for (a) [D-Arg^0,Hyp^3,Thi^5,D-Phe^7,Acc^8]BK (**1**); (b) Aaa[D-Arg^0,Hyp^3,Thi^5,D-Phe^7,Acc^8]BK (**2**); (c) [D-Arg^0,Hyp^3,Thi^{5,8},Apc^7]BK (**3**); and (d) Aaa[D-Arg^0,Hyp^3,Thi^{5,8},Apc^7]BK (**4**).

$-\Delta\delta/\Delta T$, may indicate open reverse structures, without hydrogen bonds.

Analysis of Calculations

To measure the changes in the geometries of the peptides, the root mean square deviation (RMSD) during MD simulation time was obtained (Figure 2). The RMSD changes were fitted to the Cα atoms of 'start' frame of the first trajectory specified. As seen, the changes of geometries are largest for the peptides modified with Apc at position 7 (peptides **3** and **4**). However, in the case of peptide **2** (red line), at 3.5 ns of simulations, the peptide changes considerably the conformation and displays similar tendency toward the end of the simulations. The analysis of the peptide fluctuations (Figure 3) shows that the positional fluctuations of the Cα atoms of the Arg residues at positions 2 and 9 of peptides modified with Apc (peptides **3** and **4**) are larger than in the case of peptides with Acc (peptides **1** and **2**). Moreover, the fluctuations of the Cα atoms of Gly^4 and Ser^5 in peptide **3** exceed 3 Å, in contrast to the remaining peptides.

Analysis of the radius of gyration (Rg) changes (Figure 2) shows that in the case of peptides modified with the Apc residue at position 7, the Rg decreases during MD simulations, however, the TAV distance and dihedral angle restrains had a much slighter effect on the size of peptide **3** than of peptide **4**. In turn, the Rg values for peptide **1** oscillate within 6.1–7.7 Å throughout the entire MD simulations, whereas peptide **2** exhibits the tendency to be more extended by the end of the MD simulations. Table 4 presents the radii of gyration averaged within the last of 800 ps of the MD simulations. As seen, the calculated ensemble-averaged radii of gyration indicate only very small differences in size among peptides **2**, **3**, and **4**. In turn, peptide **1** seems to be more compact than the others.

The structures of the peptides obtained during the last 800 ps of simulations, aligned to their first coordinates using Cα atoms within the common

DOI: 10.1002/psc

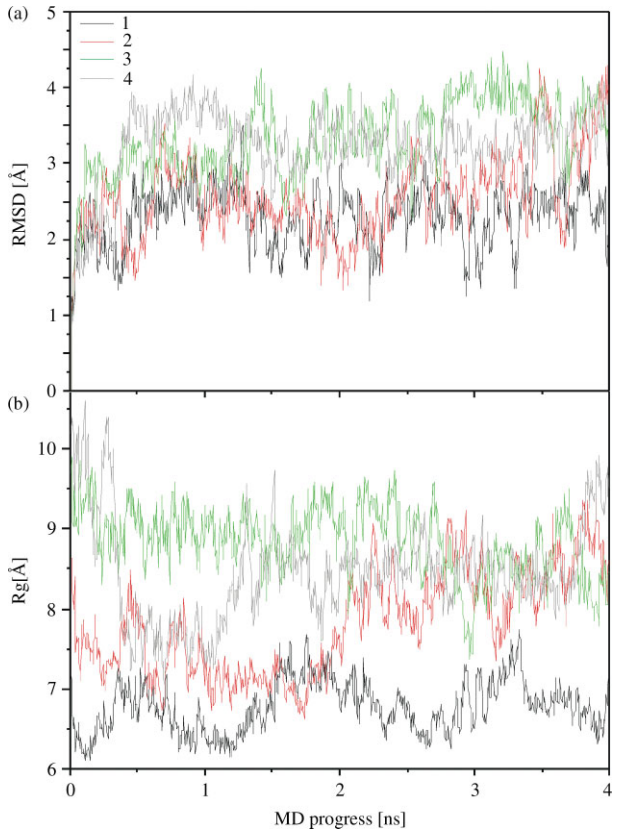

Figure 2 Root mean square deviation changes (panel a) and radius of gyration changes (panel b) of the BK antagonists in the MD simulations with TAV, where black line refers to [D-Arg^0,Hyp^3,Thi^5,D-Phe^7,Acc^8]BK (**1**); red line to Aaa[D-Arg^0,Hyp^3,Thi^5,D-Phe^7,Acc^8]BK (**2**); green line to [D-Arg^0,Hyp^3,Thi^{5,8},Apc^7]BK (**3**); and gray line to Aaa[D-Arg^0,Hyp^3,Thi^{5,8},Apc^7]BK (**4**). The changes were fitted to the Cα atoms of 'start' frame of the first trajectory specified.

D-Arg^0-Ser^6 fragment, are shown in Figure 4. The RMSD values for the ensemble of structures are collected in Table 4.

Main structural features of the peptides are bent structures (Table 4). Thi residue at position 5 promotes formation of an inverse γ-turn with Thi at top of it, closed with HN^6–CO^4 hydrogen bond, except for peptide **4**, when the inverse γ-turn is nonideal, and as a result it is not stabilized by hydrogen bond. Peptide **1** is the only one possessing the βII-turn at position 3,4 which is characteristic of BK antagonists. Moreover, about 50% of the calculated structures of peptide **1** show the tendency to create the cation-π interactions between the positively charged guanidine group of Arg^1 and aromatic ring of D-Phe^7 [58].

Acylation of the *N*-terminus with Aaa (peptides **2** and **4**) influences creation of γ-turn in Aaa^{-1}-Arg^1 stabilized by the HN^1–CO^{-1} hydrogen bond. However, in the case of peptide **2**, the changes produced by acylation are much more dramatic than those in peptide **4** (Figure 5). In contrast to peptide **1**, peptide **2** creates type II of β-turn in the Aaa^{-1}-Pro^2 fragment.

With peptide **4**, the ST-turn within the Ser^6-Thi^8 fragment was found [59]. The ST-turn consists of a hydrogen-bonded ring of nine atoms. The hydrogen bond is created between the side chain oxygen atom of Ser^6 and the main chain HN group of a residue 2 ahead (Thi^8). Among the analyzed structures of peptide **4**, over 70% of them create type I of ST-turn (Figure 6). It is also worth emphasizing, that among the peptides studied only peptide **3** is stabilized by a salt bridge between the guanidine moiety of Arg^1 and the *C*-terminal carboxyl group of Arg^9. However, the common feature of all the peptides is the position of the side chain of D-Arg^0, which lies apart from the rest of the molecule.

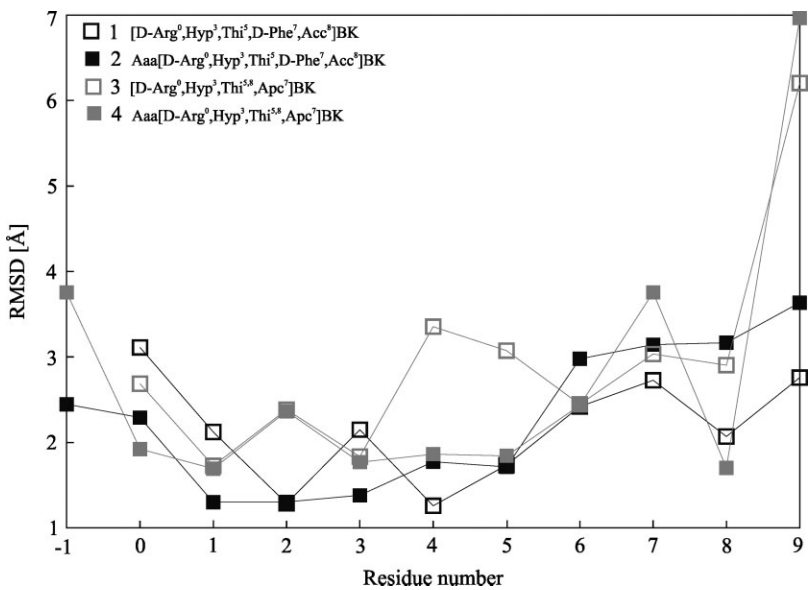

Figure 3 Variation along the polypeptide chain of the time-averaged RMSD fluctuations of the C$_\alpha$ atoms for the BK analogs in water.

DOI: 10.1002/psc

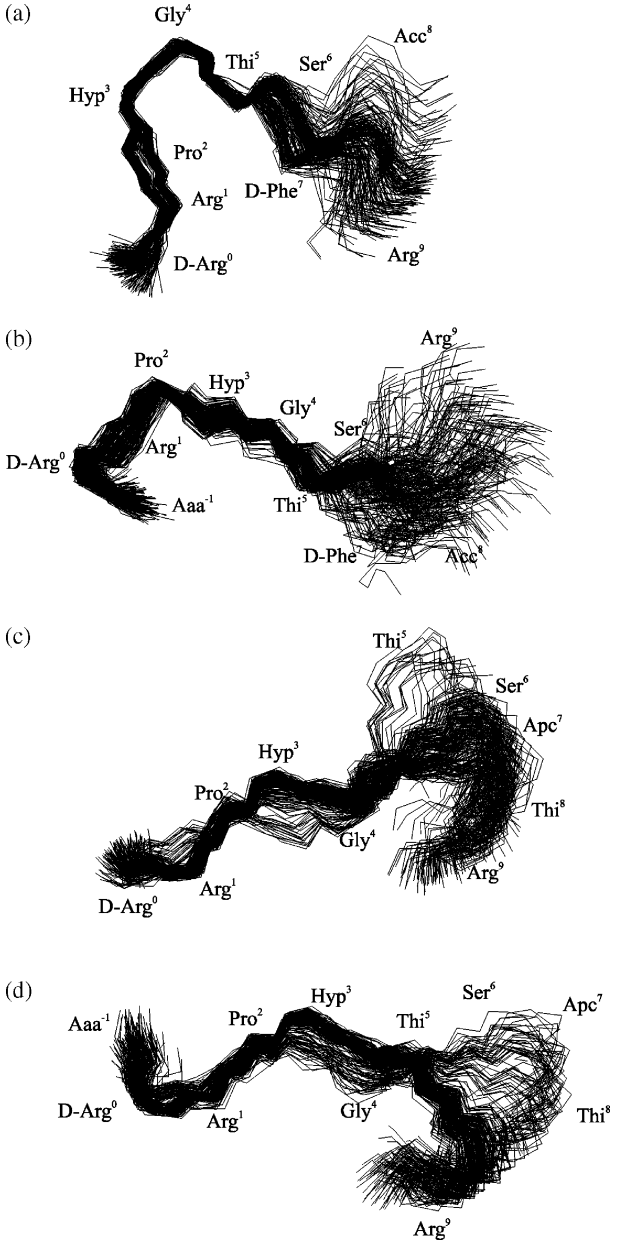

Figure 4 Superposed conformations of each peptide obtained in the last 800 ps of MD simulations with time-averaged distance and dihedral angle restraints, (a) [D-Arg^0,Hyp^3,Thi^5,D-Phe^7,Acc^8]BK (**1**); (b) Aaa[D-Arg^0,Hyp^3,Thi^5, D-Phe^7,Acc^8]BK (**2**); (c) [D-Arg^0,Hyp^3,Thi^{5,8},Apc^7]BK (**3**), and (d) Aaa[D-Arg^0,Hyp^3,Thi^{5,8},Apc^7]BK (**4**). RMSD$_{0-6}$ = 0.562, 0.878, 0.967, and 0.745 Å for C$_\alpha$ atoms, respectively.

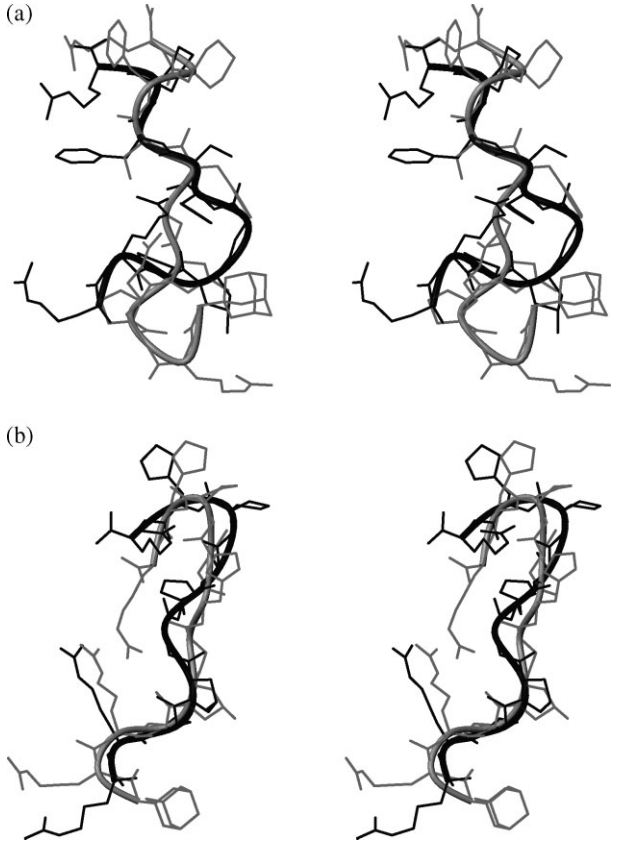

Figure 5 Stereo-view of the comparison of average conformations of [D-Arg^0,Hyp^3,Thi^5,D-Phe^7,Acc^8]BK (**1**) with Aaa[D-Arg^0,Hyp^3,Thi^5,D-Phe^7,Acc^8]BK (**2**) (a) and [D-Arg^0, Hyp^3,Thi^{5,8},Apc^7]BK (**3**) with Aaa[D-Arg^0,Hyp^3,Thi^{5,8},Apc^7]BK (**4**) (b). Gray line corresponds to the Aaa-residue acylated analogs. The average structures were extracted from the final 800 ps (200 conformers) and then minimized.

DISCUSSION

According to the results of the NMR measurements, the BK antagonists contain 7–30% of minor conformation resulting from *cis*/*trans* isomerization of the peptide bonds preceding either Pro or Hyp residues. It should be emphasized that higher percentage of a minor isomer is characteristic of peptides modified with the Apc residue at position 7 (peptides **3** and **4**). The presence of the minor isomer suggests that the peptides have no single stable conformation in aqueous solution.

Peptide **1** exhibits the strongest vasodepressor potency among the analogs and as a single one forms the βII-turn in the 2–5 fragment, which is believed to be crucial for antagonistic activity. Moreover, peptide **1** shows the tendency to create the cation-π interactions between the guanidine group of Arg^1 and aromatic ring of D-Phe^7. This peptide is also the most compact. The Rg amounts to 6.9 Å and is by *ca* 1.5 Å lower than that for the remaining analogs. Acylation of peptide **1** with Aaa moves the βII-turn toward the *N*-terminus and in peptide **2**, it appears in the Aaa^{-1}-Pro^2 fragment. This change impaired vasodepressor potency more than three times as compared to that of peptide **1**, whereas antagonistic properties in the rat uterus assay were preserved.

Conformational changes caused by acylation of peptide **3** are not so impressive (Figure 5(b)) but are essential enough to be the reason for a five-fold improvement of the vasodepressor potency at lower doses and a three-fold at higher doses. Moreover,

DOI: 10.1002/psc

Table 4 Conformational properties of the BK analogs found for conformations obtained in the last 800 ps of MD simulations with time-averaged distance and dihedral angle restraints

Peptide	Structures	Interactions	[a]RMSD$_{0-6C\alpha}$ (Å)	[b]Rg (Å)
1. [D-Arg^0,Hyp^3,Thi^5,D-Phe^7,Acc^8]BK	Hyp^3-Gly^4 β II	HN^6–CO^4	0.562	6.9
	Thi^5 γ^a			
	Acc^8 γ			
		Cation-π: Arg^1-D-Phe^7		
2. Aaa[D-Arg^0,Hyp^3,Thi^5,D-Phe^7,Acc^8]BK	D-Arg^0-Arg^1 β II		0.878	8.6
	Ser^6-D-Phe^7 β IV			
	D-Arg^0 γ	HN^1–CO^{-1}		
	Thi^5 γ^a	HN^6–CO^4		
3. [D-Arg^0,Hyp^3,Thi^{5,8},Apc^7]BK	Thi^5 γ^a	HN^6–CO^4	0.967	8.5
		Salt bridge: Arg^1-COO$^-$ Arg^9		
4. Aaa[D-Arg^0,Hyp^3,Thi^{5,8},Apc^7]BK	D-Arg^0 γ	HN^1–CO^{-1}	0.745	8.5
	Thi^5 γ^a			
	ST-turn 6–8	HN^8–OG^6		

[a] The structures of the peptides obtained during the last 800 ps of simulations aligned to their first coordinates using Cα atoms within the common D-Arg^0-Ser^6 fragment.
[b] Rg values were averaged within the last 800 ps of MD simulations.

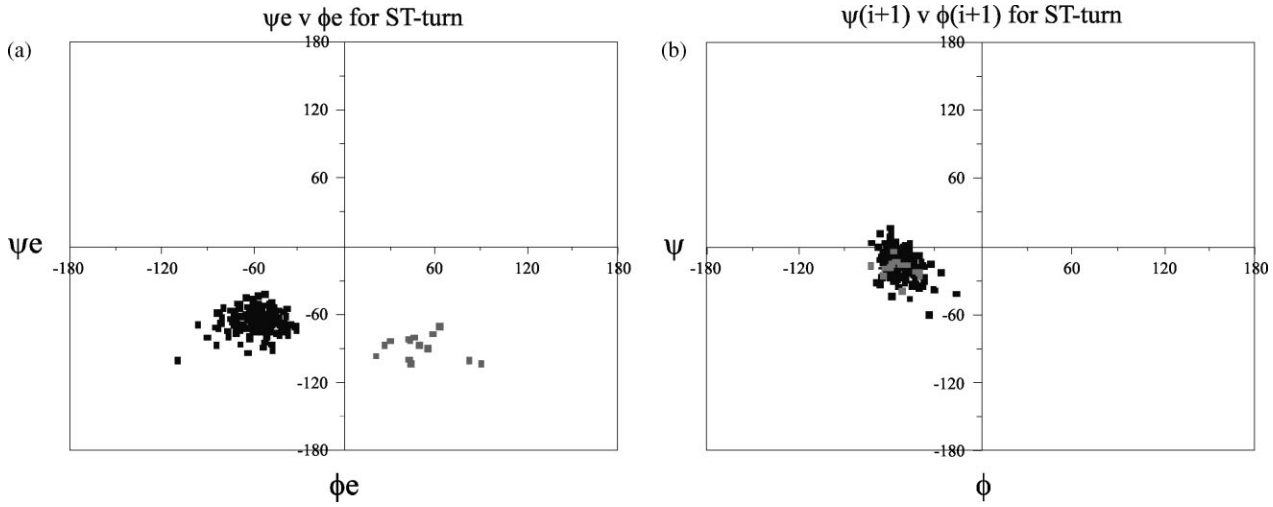

Figure 6 Types of ST-turn found for peptide **4**. $\phi e(O\gamma^i–C\beta^i–C\alpha^i–C^i)$ and $\psi e(C\beta^i–C\alpha^i–C^i–N^{i+1})$ are the angles equivalent to $\phi(i+1)$ and $\psi(i+1)$ of β-turns (a), whereas position $i+1$ of ST-turn is equivalent to $i+2$ of β-turn (b). Black color corresponds to type I ST-turn, whereas gray to type II′ ST-turn.

compound **3** exhibits negligible agonistic properties in the *in vitro* uterus assay, while compound **4** is inactive. These differences in activities may be due to the presence of the ST-turn of type I in Ser^6-Thi^8 and of the γ-turn in the Aaa^{-1}-Arg^1 fragment of peptide **4**.

None of the BK antagonists studied creates βII′-turn in the 6–9 fragment. Similar results have been obtained in our earlier investigations, i.e. the [Aca^{-1},D-Arg^0,Hyp^3,Thi^5,D-Phe^7,(*N*-Bzl)Gly^8]BK analog exhibiting strong vasodepressor potency [16] adopts type VIb of β-turn comprising residues Ser^6-Arg^9 and either the βI or βII-turn involving the Pro^2-Thi^5 fragment [60]. The presence of βVI-turn is determined by the *cis* peptide bond between D-Phe^7 and (*N*-Bzl)Gly^8. This fact suggests that *C*-terminal βII′-turn may not be crucial for antagonistic properties of the BK analogs. However, hydrophobic character of the *C*-terminus may be very important for determining B2 antagonism [61].

Summing up, we have determined three-dimensional structures of four BK antagonists. The analysis of structural differences exhibited by different modifications provides the basis for understanding conformation – activity relationships and thereby the mechanism of interactions of the analogs with receptors. Moreover, the results offer possibilities for designing new analogs with predictable biological activity.

DOI: 10.1002/psc

Acknowledgements

This work was supported by the State Committee for Scientific Research, Poland, grant nos. KBN 1108/T09/2005/28 and BW 8000-5-0457-7. The calculations were carried out in the Academic Computer Centre (TASK) in Gdańsk, Poland. Dr Adam Prahl (University of Gdańsk) is acknowledged for providing the peptides for NMR investigations.

REFERENCES

1. Eric J, Bkaily G, Bkaily GB Jr, Volkov L, Gabra BH, Sirois P. Des-Arg9-bradykinin increases intracellular Ca2+ in bronchoalveolar eosinophils from ovalbumin-sensitized and -challenged mice. *Eur. J. Pharmacol.* 2003; **475**: 129–137.
2. Steranka LR, Farmer SG, Burch RM. Antagonists of B2 bradykinin receptors. *FASEB J.* 1989; **3**: 2019–2025.
3. Bhoola KD, Figueroa CD, Worthy K. Bioregulation of kinins: kallikreins, kininogens, and kininases. *Pharmacol. Rev.* 1992; **44**: 1–80.
4. Marceau F, Regoli D. Bradykinin receptor ligands: therapeutic perspectives. *Nat. Rev. Drug Discov.* 2004; **3**: 845–852.
5. Piserchio A, Zelesky V, Yu J, Taylor L, Polgar P, Mierke DF. Bradykinin B2 receptor signaling: structural and functional characterization of the C-terminus. *Biopolymers* 2005; **80**: 367–373.
6. Margolius HS. Theodore cooper memorial lecture. Kallikreins and kinins. Some unanswered questions about system characteristics and roles in human disease. *Hypertension* 1995; **26**: 221–229.
7. Vellani V, Zachrisson O, McNaughton PA. Functional bradykinin B1 receptors are expressed in nociceptive neurones and are upregulated by the neurotrophin GDNF. *J. Physiol.* 2004; **560**: 391–401.
8. Regoli D, Barabé J. Kinin receptors. *Meth. Enzymol.* 1988; **163**: 210–230.
9. Phillips E, Conder MJ, Bevan S, McIntyre P, Webb M. Expression of functional bradykinin receptors in Xenopus oocytes. *J. Neurochem.* 1992; **58**: 243–249.
10. Stewart JM. Bradykinin antagonists: development and applications. *Biopolymers* 1995; **37**: 143–149.
11. Stewart JM, Gera L, York EJ, Chan DC, Bunn PA Jr. Structural modifications of highly potent bradykinin antagonists and their pharmacological consequences. In *Peptides 2000*, Martinez J, Fehrentz JA (eds). EDK: Paris, 2001; 945–946.
12. Stewart JM. Bradykinin antagonists: discovery and development. *Peptides* 2004; **25**: 527–532.
13. Vavrek RJ, Stewart JM. Competitive antagonists of bradykinin. *Peptides* 1985; **6**: 161–164.
14. Schachter LR, Uchida Y, Longridge DJ, Labedz T, Whalley ET, Vavrek RJ, Stewart JM. New synthetic antagonists of bradykinin. *Br. J. Pharmacol.* 1987; **92**: 851–855.
15. Stewart JM, Vavrek RJ. Bradykinin competitive antagonists for classical kinin systems. *Adv. Exp. Med. Biol.* 1986; **198**: 537–542.
16. Dawidowska O, Wierzba TH, Prahl A, Kowalczyk W, Derdowska I, Neubert K, Zabrocki J, Olejniczak B, Juzwa W, Lammek B. Potent bradykinin antagonists containing N-benzylglycine or N-benzyl-L-alanine in position 8. *J. Pept. Res.* 2004; **63**: 29–35.
17. Lee SC, Russell AF, Laidig WD. Three-dimensional structure of bradykinin in SDS micelles. Study using nuclear magnetic resonance, distance geometry, and restrained molecular mechanics and dynamics. *Int. J. Pept. Protein Res.* 1990; **35**: 367–377.
18. Kotovych G, Cann JR, Stewart JM, Yamamoto H. NMR and CD conformational studies of bradykinin and its agonists and antagonists: application to receptor binding. *Biochem. Cell Biol.* 1998; **76**: 257–266.
19. Liu X, Stewart JM, Gera L, Kotovych G. Proton magnetic resonance studies of bradykinin antagonists. *Biopolymers* 1993; **33**: 1237–1247.
20. Kyle DJ, Blake PR, Smithwick D, Green LM, Martin JA, Sinsko JA, Summers MF. NMR and computational evidence that high-affinity bradykinin receptor antagonists adopt C-terminal beta-turns. *J. Med. Chem.* 1993; **36**: 1450–1460.
21. Otter A, Bigler P, Stewart JM, Kotovych G. A proton magnetic resonance study of two synthetic agonist-antagonists pairs of bradykinin analogues. *Biopolymers* 1993; **33**: 769–780.
22. Sejbal J, Cann JR, Stewart JM, Gera L, Kotovych G. An NMR, CD, molecular dynamics, and fluorometric study of the conformation of the bradykinin antagonist B-9340 in water and in aqueous micellar solutions. *J. Med. Chem.* 1996; **39**: 1281–1292.
23. Chou PY, Fasman GD. Prediction of beta-turns. *Biophys. J.* 1979; **26**: 367–384.
24. Wilmot CM, Thornton JM. Analysis and prediction of the different types of beta-turn in proteins. *J. Mol. Biol.* 1988; **203**: 221–232.
25. Rose GD, Gierasch LM, Smith JA. Turns in peptides and proteins. *Adv. Protein Chem.* 1985; **37**: 1–109.
26. Hutchinson EG, Thornton JM. A revised set of potentials for beta-turn formation in proteins. *Protein Sci.* 1994; **3**: 2207–2216.
27. Labudda O, Wierzba T, Sobolewski D, Kowalczyk W, Śleszyńska M, Gawiński Ł, Plackowa M, Slaninová J, Prahl A. New bradykinin analogues substituted in positions 7 and 8 with sterically restricted 1-aminocyclopentane-1-carboxylic acid. *J. Pept. Sci.* 2006; **12**: 775–779.
28. Labudda-Dawidowska O, Wierzba TH, Prahl A, Kowalczyk W, Gawiński Ł, Plackova M, Slaninová J, Lammek B. New bradykinin analogues modified in the C-terminal part with sterically restricted 1-aminocyclohexane-1-carboxylic acid. *J. Med. Chem.* 2005; **48**: 8055–8059.
29. Trzeciak H, Kozik W, Melhem S, Kania A, Dobrowolski D, Prahl A, Derdowska I, Lammek B. New bradykinin analogs in contraction of rat uterus. *Peptides* 2000; **21**: 829–834.
30. Prahl A, Wierzba T, Winklewski P, Musia3 P, Juzwa W, Lammek B. Antagonists of bradykinin modified with conformationally restricted dipeptide fragment. *Pol. J. Chem.* 1997; **71**: 929–935.
31. Toniolo C, Crisma M, Valle G, Bonora GM, Polinelli S, Becker EL, Freer RJ, Sudhanand R, Rao RB, Balaram P, Sukumar M. Conformationally restricted formyl methionyl tripeptide chemoattractants: a three-dimensional structure-activity study of analogs incorporating a C alpha,alpha-dialkylated glycine at position 2. *Pept. Res.* 1989; **2**: 275–281.
32. Toniolo C, Benedetti E. Structures of polypeptides from α-amino acids disubstituted at the α-carbon. *Macromolecules* 1994; **24**: 4004–4009.
33. Paul PKC, Sukumar M, Bardi R, Piazzesi AM, Valle G, Toniolo C, Balaram P. Stereochemically constrained peptides. Theoretical and experimental studies on the conformations of peptides containing 1-aminocyclohexanecarboxylic acid. *J. Am. Chem. Soc.* 1986; **108**: 6363–6370.
34. Paradisi M, Torrini I, Zecchini GP, Luente G, Gauvuzzo E, Mazza F, Pochetti G. γ-Turn conformation induced by α,α-disubstituted amino acids with a cyclic six-membered side chain. *Tetrahedron* 1995; **51**: 2379–2386.
35. Bax A, Davies DG. MLEV-17 based two-dimensional homonuclear magnetization transfer spectroscopy. *J. Magn. Reson.* 1985; **65**: 355–360.
36. Kumar A, Ernst RR, Wüthrich K. A two-dimensional nuclear Overhauser enhancement (2D NOE) experiment for the elucidation of complete proton-proton cross-relaxation networks in biological macromolecules. *Biochim. Biophys. Res. Commun.* 1980; **95**: 1–6.
37. Bothner-By AA, Stephens RL, Lee JM, Warren CD, Jeanloz RW. Structure determination of a tetrasaccharide: transient nuclear Overhauser effects in the rotating fram. *J. Am. Chem. Soc.* 1980; **106**: 811–813.
38. Bax A, Davis DG. Practical aspects of two-dimensional transverse NOE spectroscopy. *J. Magn. Reson.* 1985; **63**: 207–213.

39. Kay LE, Keifer P, Saarinen T. Pure absorption gradient enhanced heteronuclear single quantum correlation spectroscopy with improved sensitivity. *J. Am. Chem. Soc.* 1992; **114**: 10663–10665.
40. Kontaxis G, Stonehouse J, Laue ED, Keeler J. The sensitivity of experiments which use gradient pulses for coherence-pathway selection. *J. Magn. Reson. A* 1994; **111**: 70–76.
41. Bax A, Summers MF. Proton and carbon-13 assignments from sensitivity-enhanced detection of heteronuclear multiple-bond connectivity by 2D multiple quantum NMR. *J. Am. Chem. Soc.* 1986; **108**: 2093–2094.
42. Rance M, Sorensen OW, Bodenhausen G, Wagner G, Ernst RR, Wüthrich K. Improved spectral resolution in cosy 1H NMR spectra of proteins via double quantum filtering. *Biochem. Biophys. Res. Commun.* 1983; **117**: 479–485.
43. Wishart DS, Bigam CG, Holm A, Hodges RS, Sykes BD. 1H, 13C and 15N random coil NMR chemical shifts of the common amino acids. I. Investigations of nearest-neighbor effects. *J. Biomol. NMR* 1995; **5**: 67–81.
44. Varian, Nuclear Magnetic resonance Instruments, VnmrTM Software, Revision 5.3B 1/97.
45. Bartles C, Xia T, Billeter M, Günter P, Wütrich K. The program XEASY for computer-supported NMR spectral analysis of biological macromolecules. *J. Biomol. NMR* 1995; **5**: 1–10.
46. Case DA, Darden TA, Cheatham TE III, Simmerling CL, Wang J, Duke RE, Luo R, Merz KM, Wang B, Pearlman DA, Crowley M, Brozell S, Tsui V, Gohlke H, Mongan J, Hornak V, Cui G, Beroza P, Schafmeister C, Caldwell JW, Ross WS, Kollman PA. *AMBER 8*. University of California: San Francisco, 2004.
47. Allen FH, Davies JE, Galloy JJ, Johnson O, Kennard O, Macrae CF, Mitchell EM, Mitchell GF, Smith JM, Watson DG. The development of versions 3 and 4 of the Cambridge structural database system. *J. Chem. Inf. Comput. Sci.* 1991; **31**: 187–204.
48. Schmidt MW, Baldridge KK, Boatz JA, Elbert ST, Gordon MS, Jensen JH, Koseki S, Matsunaga N, Nguyen KA, Su S, Windus TL, Dupuis M, Montgomery JA. General atomic and molecular electronic structure system. *J. Comput. Chem.* 1993; **14**: 1347–1363.
49. Bayly CI, Cieplak P, Cornell WD, Kollman PA. A well-behaved electrostatic potential based method using charge restraints for deriving atomic charges: the RESP model. *J. Phys. Chem.* 1993; **97**: 10269–10280.
50. Güntert P, Mumenthaler C, Wüthrich K. Torsion angle dynamics for NMR structure calculation with the new program DYANA. *J. Mol. Biol.* 1997; **273**: 283–298.
51. Bolton PH, Carlson RMK, Croasmun WR, Crouch RC, Dabrowski J, Dyson HJ, Goljer I, Gray GA, Griesinger C, Hull WH, Kalbitzer HR, Kessler H, Martin GE, Rinaldi PL, Sattler M, Schleucher J, Schwalbe H, Seip S, Wright PE. *Two-dimensional NMR Spectroscopy: Applications for Chemists and Biochemists*, Croasmun WR, Carlson RMK (eds). VCH: New York, 1994.
52. Pardi A, Billeter M, Wüthrich K. Calibration of the angular dependence of the amide proton-C alpha proton coupling constants, 3JHN alpha, in a globular protein. Use of 3JHN alpha for identification of helical secondary structure. *J. Mol. Biol.* 1984; **180**: 741–751.
53. Koradi R, Billeter M, Wüthrich K. MOLMOL: a program for display and analysis of macromolecular structures. *J. Mol. Graph.* 1996; **14**: 52–55.
54. Hill JM, Alewood PF, Craik DJ. Three-dimensional solution structure of mu-conotoxin GIIIB, a specific blocker of skeletal muscle sodium channels. *Biochemistry* 1996; **35**: 8824–8835.
55. Dyson HJ, Rance M, Houghten RA, Lerner RA, Wright PE. Folding of immunogenic peptide fragments of proteins in water solution. II. The nascent helix. *J. Mol. Biol.* 1988; **201**: 161–200.
56. Wüthrich K, Billeter M, Braun W. Polypeptide secondary structure determination by nuclear magnetic resonance observation of short proton-proton distances. *J. Mol. Biol.* 1984; **180**: 715–740.
57. Bach AC II, Eyerman CY, Gross JD, Bower MJ, Haflow RL, Weber PC, Degrado WF. Structural studies of a family of high affinity ligands for GPIIb/IIIa. *J. Am. Chem. Soc.* 1994; **116**: 3207–3219.
58. Gallivan JP, Dougherty DA. Cation-pi interactions in structural biology. *PNAS* 1999; **96**: 9459–9464.
59. Duddy WJ, Nissink JWM, Allen FH, Milner-White EJ. Mimicry by asx- and ST-turns of the four main types of beta-turn in proteins. *Protein Sci.* 2004; **13**: 3051–3055.
60. Sikorska E, Olusarz R, Lammek B. Conformational studies of two bradykinin antagonists by using two-dimensional NMR techniques and molecular dynamics simulations. *J. Biomol. Struct. Dyn.* 2005; **23**: 125–134.
61. Miskolzie M, Gera L, Stewart JM, Kotovych G. The importance of the N-terminal beta-turn in bradykinin antagonists. *J. Biomol. Struct. Dyn.* 2000; **18**: 249–260.